The Astrophysical Journal, 947:78 (10pp), 2023 April 20 https://doi.org/10.3847/1538-4357/acbdf6

Observation of the Hall Magnetic Reconnection As Close As 56 Solar Radii from the Sun

Rongsheng Wang[1,2,3], Xiancai Yu[4], Yuming Wang[1,2], Quanming Lu[1,2,3], and San Lu[1,2,3]
[1] Deep Space Exploration Laboratory/School of Earth and Space Sciences, University of Science and Technology of China, Hefei, 230026, People's Republic of China; rswan@ustc.edu.cn
[2] CAS Center for Excellence in Comparative Planetology/CAS Key Laboratory of Geospace Environment/Anhui Mengcheng National Geophysical Observatory, University of Science and Technology of China, Hefei, 230026, People's Republic of China
[3] Collaborative Innovation Center of Astronautical Science and Technology, Harbin, People's Republic of China
[4] Beijing Key Laboratory of Space Environment Exploration, National Space Science Center, Chinese Academy of Sciences, Beijing, 100190, People's Republic of China
Received 2022 December 8; revised 2023 February 17; accepted 2023 February 20; published 2023 April 25

Abstract

A few thin current layers were detected in the rear boundary of an interplanetary coronal mass ejection (ICME) observed at 56 solar radii from the Sun as the Parker Solar Probe spacecraft approached the perihelion for the first time, and were caused by the interaction between the background solar wind and the rear boundary of the ICME. Among two of the current layers, the ion diffusion region of the Hall magnetic reconnection was directly detected, based on opposite ion jets, low-speed inflows, and the Hall effect. Both reconnection events were fast and occurred in the current layer with a small magnetic field shear angle and with significantly asymmetric magnetic field intensity as well as plasma between their two sides, i.e., an asymmetric magnetic reconnection with a strong guide field. A magnetic flux rope was detected inside one of the diffusion regions, indicating bursty reconnection. Additionally, multiple reconnection jets were detected inside the ICME and its rear boundary. Thus, we speculate that more ongoing reconnection events were occurring inside the ICME and its boundary. The observations suggested that fast Hall magnetic reconnection can occur as close as 56 solar radii from the Sun and plays a crucial role in ICME evolution.

Unified Astronomy Thesaurus concepts: Solar wind (1534); Heliosphere (711)

1. Introduction

Interplanetary coronal mass ejections (ICMEs), as interplanetary manifestations of solar coronal mass ejections, have been extensively investigated and are found to play a key role in solar–terrestrial interactions (Wang et al. 2002; Alexander et al. 2006; Gopalswamy 2006; Zhang et al. 2007; Chen 2011; Shen et al. 2017). As a subset of ICMEs, magnetic clouds are generally characterized by a large smooth rotation of magnetic field, a significant enhanced magnetic strength, and a low plasma temperature as well as low plasma beta (Burlaga et al. 1981; Wang et al. 2003; Wei et al. 2006; Vörös et al. 2021). Namely, the magnetic topology of a magnetic cloud consists of a large-scale twisted magnetic flux rope and the plasma inside the rope is frequently depleted (e.g., Burlaga et al. 1981). The two ends of the flux rope root on the Sun, and thus the field-aligned counterstreaming electrons can be detected frequently inside the rope. As for fast magnetic clouds, a shock is generated at their leading edge and a compressed turbulent sheath region is generated between the shock and the flux rope. Due to their southward magnetic field component, magnetic clouds cause direct coupling of a solar-terrestrial magnetosphere via magnetic reconnection (Wang et al. 2002; Zhang et al. 2007; Lavraud et al. 2014; Y. M. Wang et al. 2018).

Once they are ejected away from the solar corona, magnetic clouds expand and propagate toward the external heliosphere and interact with the ambient magnetized plasma in various ways, resulting in complicated boundary layers (Wei et al. 2006; Zurbuchen & Richardson 2006; Vörös et al. 2021). A few magnetic clouds would interact with each other and cause complicated multiple magnetic clouds (Wang et al. 2002, 2003), which could cause great geomagnetic storms (Wang et al. 2005; Xue et al. 2005; Xiong et al. 2007; Shen et al. 2011). By estimating the accumulated azimuthal magnetic fluxes of magnetic clouds, the fluxes at the rear boundary generally exceed the fluxes at the leading part (Dasso et al. 2006; Ruffenach et al. 2012; Lavraud et al. 2014). This indicates that the fluxes at the leading part of magnetic clouds are progressively peeled by magnetic reconnection as they are propagating in the heliosphere. The evolution of magnetic clouds in the heliosphere was further explored recently using an excellent event (Y. M. Wang et al. 2018). In this event, the magnetic cloud flux rope was repeatedly encountered four times by several satellites near Mercury, Venus, Earth, and Mars. Its axial magnetic flux and helicity decreased whereas its twist increased as the flux rope propagated outward. The observations clearly show that the cloud was significantly eroded. This indicates that magnetic reconnection plays a key role in the evolution of magnetic clouds (R. S. Wang et al. 2018).

Magnetic reconnection in a current sheet can efficiently convert the stored magnetic free energy into plasma kinetic energy and heating, and accounts for many explosive phenomena in space (Vasyliunas 1975; Sonnerup 1979; Ji et al. 2022; Lu et al. 2022), e.g., solar flare and terrestrial magnetic storms. Observations in the terrestrial magnetosphere show that the reconnection is generally bursty (Nakamura et al. 2004; Wang et al. 2016; Fu et al. 2017; Li et al. 2022) and the diffusion region where the charged particles are decoupled from magnetic field lines is the key region for the occurrence of magnetic reconnection (Vasyliunas 1975; Sonnerup 1979). The characteristic of the ion diffusion region is the Hall electric field

directed toward the middle plane at both sides and the quadrupolar structure of the Hall magnetic field (Sonnerup 1979; Eastwood et al. 2010). In interplanetary space, reconnection exhausts have been commonly detected at various radii from the Sun and in the different environments (Wei et al. 2003; Gosling et al. 2005; Davis et al. 2006; Wei et al. 2006; Lavraud et al. 2009; Tian et al. 2010; Xu et al. 2011; Gosling 2012; Mistry et al. 2017; Phan et al. 2020; Voros et al. 2021), e.g., small-scale current sheets, interplanetary current sheets, and magnetic cloud boundary layers. Based on magnetospheric multiscale mission (MMS) measurements (Burch et al. 2016) in a time resolution of as high as tens of milliseconds, the reconnection diffusion region was well resolved recently in interplanetary space at ∼1 astronomical unit (au). The observation shows that the reconnection at 1 au is bursty and turbulent in the solar wind (Wang et al. 2023). In addition, a few observations at a solar radial distance of 29.5–107 solar radii (R_S) show chains of large bulges with a spatial scale up to several R_S in the reconnection exhausts (Phan et al. 2020, 2021). This suggests that bursty reconnection could occur close to the Sun in solar wind. However, there has been no direct evidence of the reconnection diffusion region there so far.

In this article, we present in situ observations of the reconnection diffusion regions in the solar wind as close as $56R_S$ from the Sun. The reconnection diffusion region was observed in the interacting region between one ICME and the background solar wind. This article is organized as follows. Section 2 displays the instrumentation and database. Section 3 presents an overview of the event. Section 4 discusses the diffusion region. Finally, Section 5 presents the discussion and conclusions.

2. Instrumentation and Database

NASA's Parker Solar Probe (PSP) was launched on 2018 August 12 and was designed to study local transient processes close to the Sun in the solar wind, including magnetic reconnection therein (Fox & McComas 2016). The data from several instruments onboard PSP are used in this article. Magnetic field data are taken from the FIELDS fluxgate magnetometer (Bale et al. 2016) and the time resolution was ∼0.43 s. The proton data are measured by SWEAP/SPC (Kasper et al. 2016; Case et al. 2020) and the time resolution is 0.9 s, which is appropriate to investigate the reconnection ion diffusion region in the solar wind. The time resolution of the electron pitch angle data taken from the SWEAP/SPAN instrument is about 28 s (Kasper et al. 2016; Whittlesey et al. 2020). The first perihelion passage is on 2018 November 6 and the closest distance is $35.4R_s$ from the Sun center.

3. Overview of a Magnetic Cloud

As the PSP spacecraft approached the perihelion for the first time, the primary science collection at a high rate occurred during the encounter phase of its orbit at less than $54R_s$ (Kasper et al. 2019). Encounter 1 lasted from 2018 October 31 to November 12 and a clear ICME was encountered during 01:00–09:00 UT on October 31, as displayed in Figure 1. The plasma data in high-time resolution were available starting at ∼05:00 UT. The magnetic field magnitude and three components in the heliocentric radial–tangential–normal (RTN) coordinates, where R is the radial direction from the Sun center to the spacecraft, T is the cross-product of the Sun's spin axis with R, and N completes the right-hand system ($N = R \times T$), are displayed in Figures 1(a) and (b), respectively. The magnetic field in the RTN spherical coordinates are shown in Figures 1(c) and (d) where the azimuthal angle (ϕ) is zero in the radial direction away from the Sun and the latitude angle (θ) is positive north of the ecliptic plane.

During the interval of 02:30∼08:00 UT, $|B|$ gradually increased (black trace in Figure 1(a)). Afterward, $|B|$ decreased quickly with a few large dips between two vertical dashed lines. In the whole interval, magnetic fluctuations were strong (Figure 1(b)) in all three components and B_N fluctuated most intensely at ∼04:00 and ∼08:00 UT, which can be obtained from its standard deviation as well (blue trace in Figure 1(a)). During 04:00–08:00 UT, B_T gradually changed signs twice from primarily positive prior to 06:30 UT to negative and then became positive again at ∼07:30 UT, while B_R and B_N were always negative (Figure 1(b)), in accord with the angle evolution where the azimuthal angle varied around ∼180° (Figure 1(c)) and the latitude angle gradually increased and then decreased (Figure 1(d)). Overall, the magnetic field smoothly rotated inside the magnetic cloud but with a few short jumps at one or more components of magnetic field, e.g., at ∼05:51, 06:08, 06:43, and 07:30 UT. In this interval, the magnetic field strength was enhanced (Figure 1(a)) and the plasma density (Figure 1(g)) and plasma beta (Figure 1(e)) declined. Just around the B_T rotation, the field-aligned bidirectional electrons at energy 314 eV continuously appeared (Figure 1(k)) during 06:00–07:45 UT. Therefore, we concluded that a magnetic cloud was encountered by PSP (Figure 6(a)). This small-scale ICME has been identified previously by Zhao et al. (2020).

Considering the field-aligned bidirectional electrons were only observed around the cloud center, we suggest this cloud had interacted profoundly with the background plasma, leading to the loss of the field-aligned bidirectional electrons in the boundary. The field-aligned bidirectional electrons around the cloud center suggest that this cloud should originate from the Sun. However, the imaging data did not show any CME event from the Sun at that time. One potential reason is that the temporal/spatial scale of this cloud was too small to be detected. The intense fluctuations of magnetic field at 02:30–04:00 and 08:15–08:38 UT correspond to the leading and rear boundary of the cloud, respectively. Here, we only studied the rear boundary because the data in high-time resolution are unavailable in the leading boundary. Inside the magnetic cloud, the electrons were heated slightly (the main population has a wider energy range, as shown in Figure 1(j)), the proton temperature was nearly constant (Figure 1(h)), and the pressure was dominated by magnetic field pressure (Figure 1(i)).

At the rear boundary of the cloud between 08:15 and 08:38 UT, all three components of magnetic field abruptly changed sign multiple times (marked by two vertical dashed lines in Figure 1), and the azimuthal as well as latitude angles dramatically varied accordingly. At least one component of magnetic field changed sign rapidly, indicating a thin current layer exists therein. These observations suggest a complicated magnetic topology at the rear boundary. Moreover, the solar wind speed was significantly enhanced, the density displayed large variation, the ion temperature was substantially raised, and thus the proton beta was bigger than 0.5. The average solar

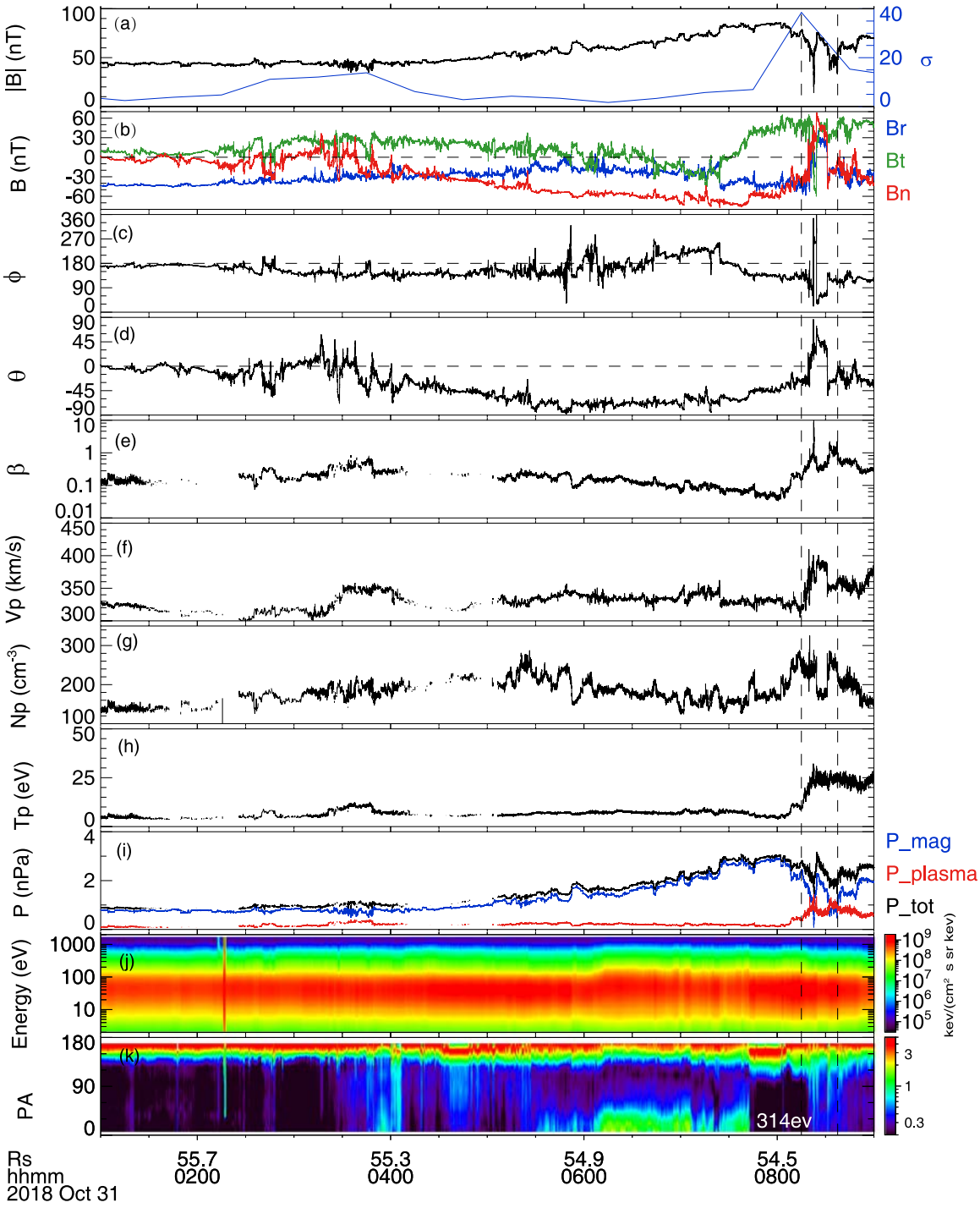

Figure 1. An overview of one magnetic cloud encountered by PSP during Encounter 1. (a) Magnetic field magnitude (black) and the standard deviation of B_N (blue), (b) magnetic field vector in the RTN coordinates, (c) azimuthal angle, (d) latitude angle, (e) plasma beta, (f) proton bulk flow speed, (g) plasma number density, (h) proton temperature, (i) magnetic pressure (blue trace), plasma pressure (red trace), and total pressure (black trace), (j) proton energy spectrum, and (k) the pitch angle distribution of the electrons at energy 314 eV.

wind speed in the rear boundary was larger than the speed inside the cloud, which would compress the cloud and created the interaction region.

Figure 2 shows the details in the rear boundary. The sharp changes of the magnetic field were observed in four short time periods labeled by the vertical shadow area. In all these short periods, azimuthal and latitude angles varied greatly (Figures 2(b) and (c)), and the plasma density (Figure 2(h)) and solar wind speed (Figure 2(d)) were enhanced significantly. Figures 2(e)–(g) display three components of magnetic field (black curves) and plasma bulk flow (red curves). The highly correlated variation of magnetic field and proton velocity is consistent with the expected Alfvén waves propagating away from the Sun. Nevertheless, the larger-amplitude variation of the flow and magnetic field associated with the density enhancement in the identified thin current layers (marked by the vertical shadow) indicates that some kinetic processes happened inside the Alfvénic fluctuations (e.g., Bale et al.

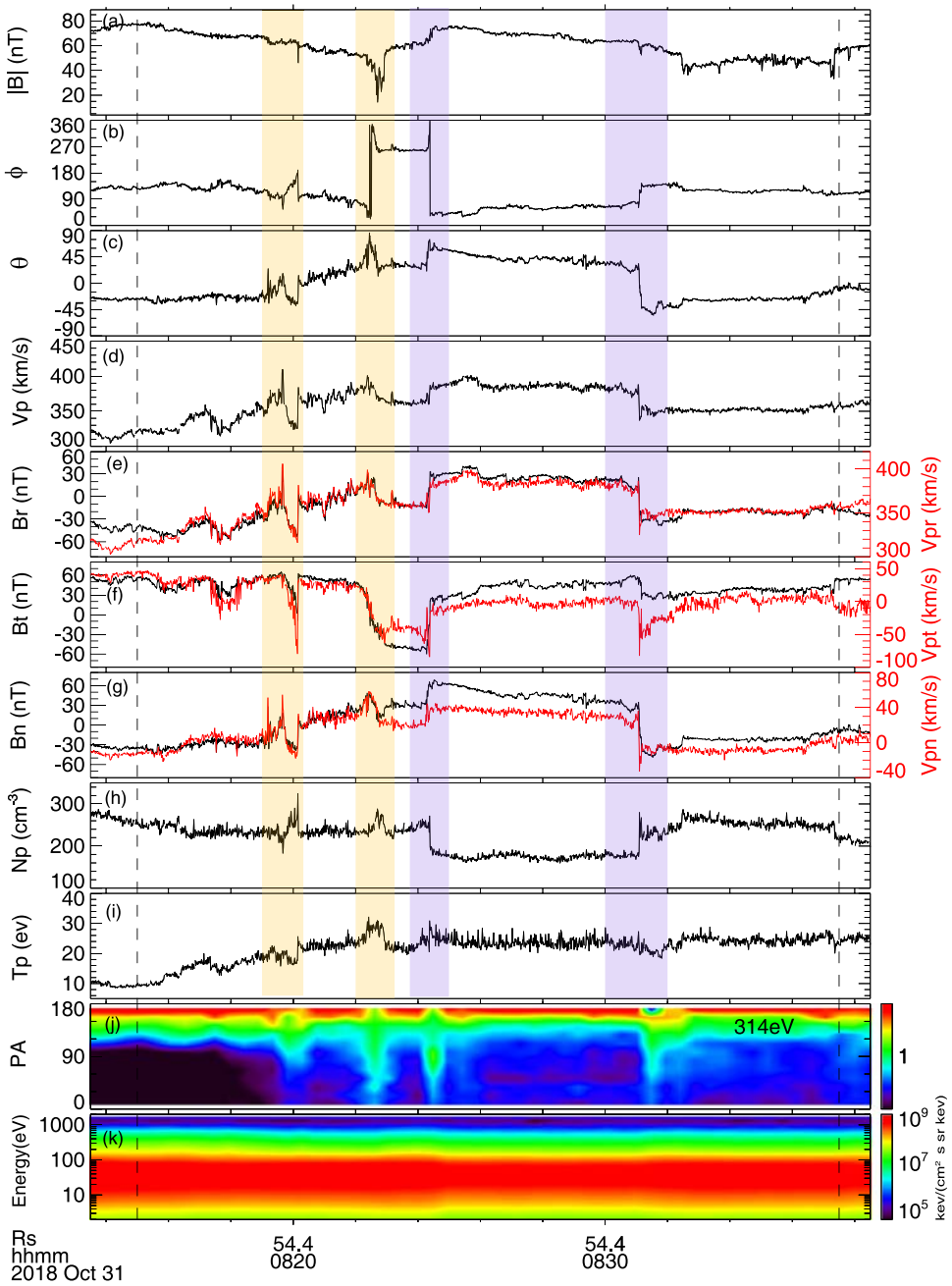

Figure 2. Observation of a few thin current layers in the rear boundary of the magnetic cloud. (a) Magnetic field magnitude, (b) azimuthal angle, (c) latitude angle, (d) proton bulk flow speed, (e)–(g) magnetic field components (black) and proton velocity components (red), (h) proton number density, (i) proton temperature, (j) electron pitch angle distribution at 314 eV, and (k) electron time–energy spectrum.

2019; Kasper et al. 2019). The electrons were slightly heated (Figure 2(k)) near the last two current layers (purple shadow) and were not explored in detail due to the low sampled rate.

A few plasma jets have been reported inside this ICME at ∼07:00 UT, and one sub-Alfvénic reconnection outflow was radial antisunward while another one was radial sunward (Phan et al. 2020). Moreover, both events have a strong guide field, larger than 1. Unfortunately, the reconnection diffusion region was not directly encountered by PSP in these events. Similar jets were detected in the ICME boundary as well, e.g., at ∼08:20 UT, marked by the first vertical yellow bar in Figure 2 and enlarged in Figure 3. The short jets were detected at ∼08:19:40 and ∼08:20:10 UT (the shadow areas in Figure 3). The jet speed exceeded 40 km s^{-1} (Figure 3(b)) and mainly in the R and N directions for the first jet and primarily in the T direction for the second jet (Figure 3(d)). The magnetic field intensity (Figure 3(a)) and proton density (Figure 3(e)) during the first jet were nearly constant while the intensity was substantially depressed and the density as well as the proton temperature rose significantly in the second jet. The duration of the two jets was only about 5 s and thus both jets were very narrow. The electron distribution inside the jets could not be explored here (Figure 3(g)). These jets could be caused by reconnection and the reason for the differences between the two jets were unclear. The observations suggest that reconnection outflow jets frequently occurred inside the ICME. Except for the jets, the reconnection diffusion region was observed in the last two current layers and is studied in the following section.

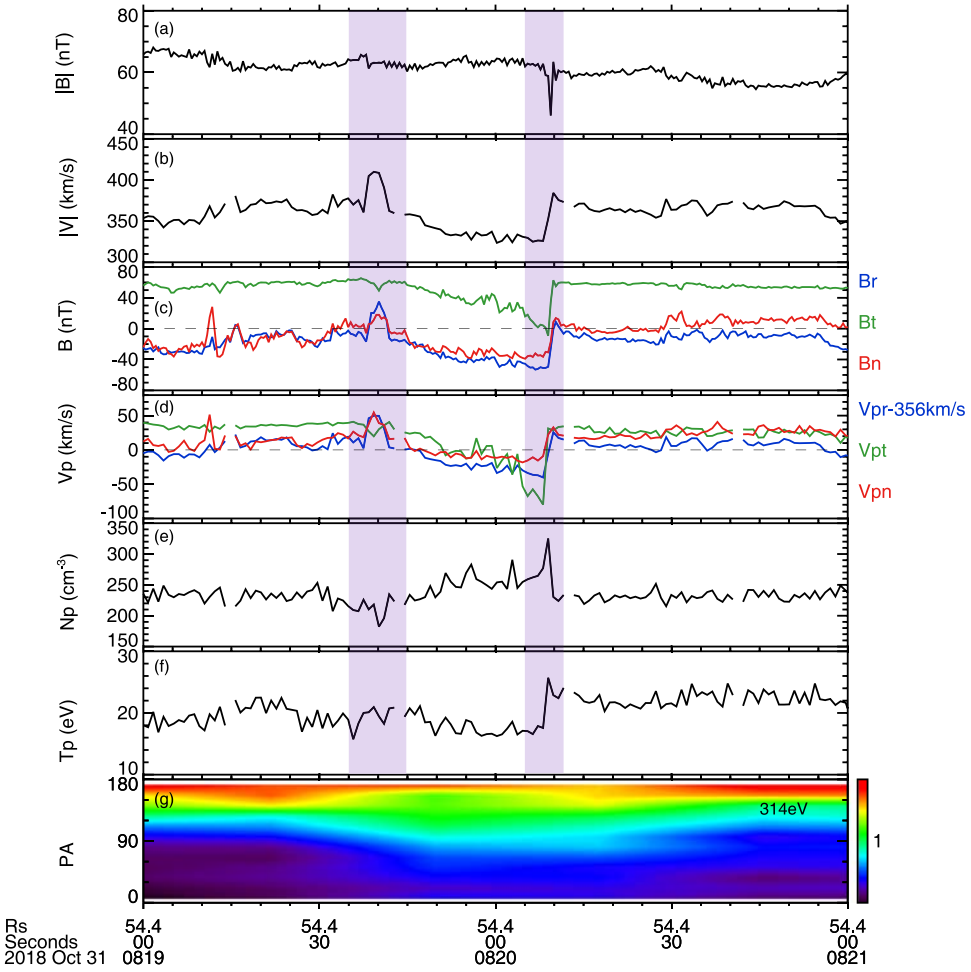

Figure 3. Plasma jets at the rear boundary of the magnetic cloud. (a) Magnetic field magnitude, (b) proton bulk flow speed, (c) magnetic field components, (d) proton velocity components, (e) proton density, (f) proton temperature, and (g) electron pitch angle distribution.

4. Reconnection Ion Diffusion Regions

At ∼08:24:20 UT, the azimuthal angle decreased abruptly from 360° to 180°, then to ∼40°, and the latitude angle changed sharply ($\delta\ \theta \approx 45°$; the third vertical purple bar in Figure 2). Thus, a thin current layer was observed there. The data in this short interval (the third vertical shaded area in Figure 2) are enlarged in Figure 4 and is displayed in the local current coordinate system with $\boldsymbol{L} = [0.457, 0.825, 0.332]$, $\boldsymbol{M} = [-0.095, 0.416, -0.904]$, and $\boldsymbol{N} = [-0.884, 0.382, 0.269]$ relative to the RTN coordinates. The normal direction $\boldsymbol{N}$ was determined from $\boldsymbol{B}_1 \times \boldsymbol{B}_2 / |\boldsymbol{B}_1 \times \boldsymbol{B}_2|$, where $\boldsymbol{B}_1$ and $\boldsymbol{B}_2$ were the magnetic field vectors at 08:23:40 and 08:25:00 UT, the two edges of the current sheet. $\boldsymbol{M} = \boldsymbol{N} \times \boldsymbol{L}'$ was approximately the out-of-plane X-line direction, where $\boldsymbol{L}'$ was the maximum variance direction from minimum variance analysis (MVA) for the magnetic field during 08:24:15–08:24:24 UT (Sonnerup & Cahill 1967), and $\boldsymbol{L} = \boldsymbol{M} \times \boldsymbol{N}$ completes the right-hand system. The result from the minimum variance analysis was nearly constant when we changed the time interval of the current layer.

B_L varied from −40 nT at ∼08:24:00 UT to 60 nT at 08:24:25 UT (Figure 4(b)), which indicates that PSP crossed the current layer from one side to the other. In this crossing, the magnetic field strength increased from ∼60 to ∼70 nT (Figure 4(a)) and the density decreased quickly from 240 to 180 cm^{-3}. Namely, the current layer was asymmetrical. The guide field was strong in this event and its value was about 50 nT, nearly equal to B_L at the edge of the current layer. The shear angle of the magnetic field between two sides of the current layer ($\arccos(\boldsymbol{B}_1 \cdot \boldsymbol{B}_2/(|\boldsymbol{B}_1| \cdot |\boldsymbol{B}_2|))$) was assessed at ∼90°.

In order to show three components of the flows clearly inside one panel, Figure 4(c) shows v_{pM} and v_{pN} minus their background flows and v_{pL} plus −135 km s^{-1}. The background flow was ∼ −75 km s^{-1} in the M direction and ∼−332 km s^{-1} in the N direction. In the downside ($B_L < 0$, prior to 08:24:15 UT) and upside ($B_L > 0$, after 08:24:25 UT) of the current layer, the background flow of v_{pL} was ∼135 and ∼175 km s^{-1}, respectively. This means a shear flow in the L direction across the current layer. Assuming this shear flow varied smoothly across the layer, this shear flow corresponded to the background flow (blue dashed curve). One remarkable feature in this layer was the opposite proton jets, relative to the background flow (Figure 4(c)). The positive jet was first detected and its maximum value was up to 40 km $s^{-1} \sim 0.6 v_A$ at ∼08:24:17 UT, where $v_A = 73$ km s^{-1} was Alfvén speed based on the asymmetric condition of the current layer, and was immediately followed by a negative jet with a speed close to 40 km s^{-1} at ∼08:24:22 UT. The flow of the jets reversed gradually and the reversal point was somewhat earlier than the B_L reversal point. The opposite sub-Alfvénic flows inside the current layer were consistent with the reconnection

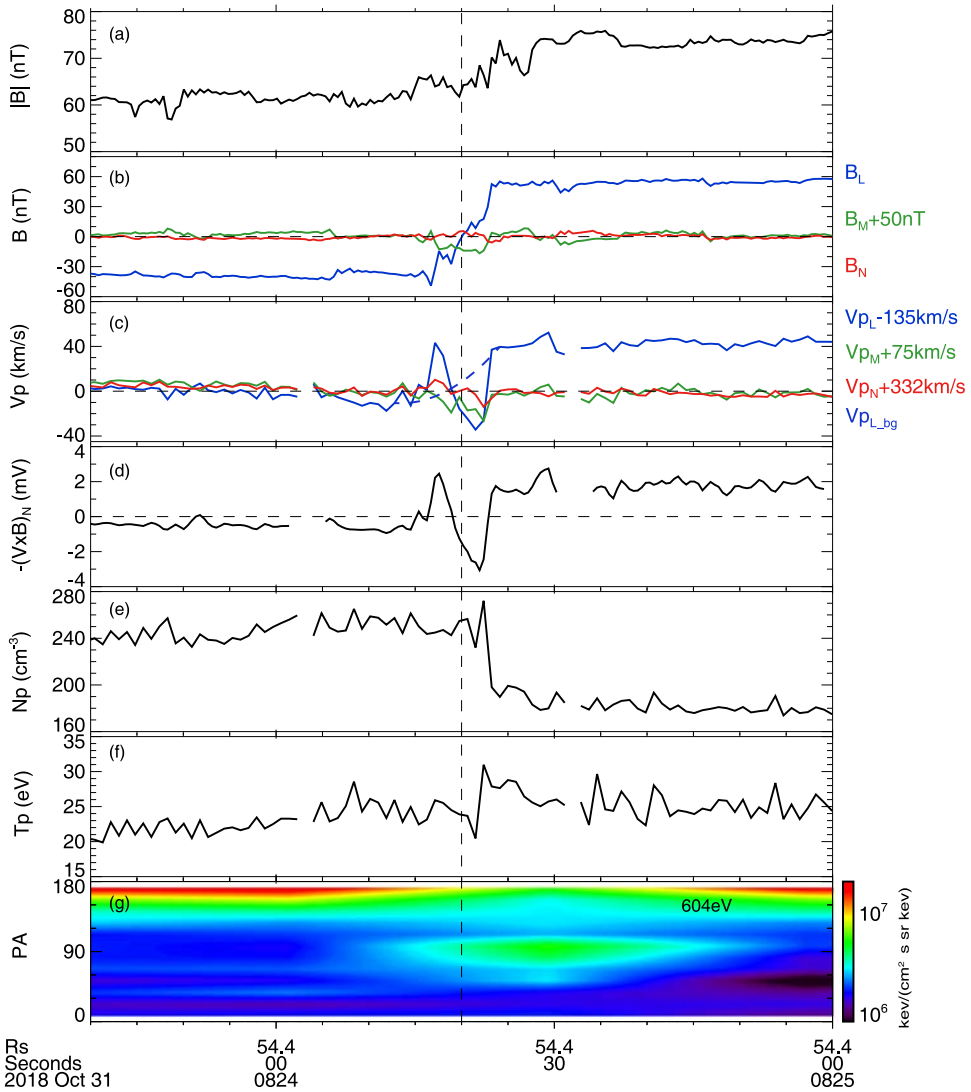

Figure 4. Ion diffusion region detected inside one thin current layer. (a) Magnetic field magnitude, (b) magnetic field components, (c) proton velocity components in the local current system, (d) electric field $-(\boldsymbol{V}\times\boldsymbol{B})_N$, (e) proton density, (f) proton temperature, and (g) electron pitch angle distribution at 604 eV.

bidirectional outflows (Nagai et al. 2001; Oieroset et al. 2001; Davis et al. 2006; Wei et al. 2006; Wang et al. 2017). This indicates that reconnection was occurring inside the current layer.

Inside the opposite flows, B_M was always negative respective to the background value and the negative enhancement of B_M was about 10 nT, ∼20% of B_L at the current layer edge, consistent with the Hall magnetic field in the left lower and right upper quadrants (Figure 6(b)) of the reconnection ion diffusion region. The Hall electric field in the N direction $-(\boldsymbol{V}\times\boldsymbol{B})_N$ was positive below the middle plane of the current layer and negative above the middle plane (Figure 4(d)). In other words, the electric field was directed to the middle plane, in good agreement with the Hall electric field (e.g., Oieroset et al. 2001; Eastwood et al. 2010). In simultaneous observations of the opposite outflows, the Hall electric field and magnetic field inside the current layer clearly show that one ion diffusion region of magnetic reconnection was observed by PSP during 08:24:15–08:24:25 UT. Inside the ion diffusion region, the proton temperature was slightly enhanced (Figure 4(f)) and energized electrons with energy up to 604 eV were measured at ∼90° (Figure 4(g)). This indicates that the plasma was significantly heated inside the ion diffusion region. However, the time resolution of the electron data (28 s) is longer than the duration of the ion diffusion region (10 s). Thus, the electron behavior inside the diffusion region cannot be well resolved here. Nevertheless, the ∼90° flux enhancement is in good agreement with recent observation in the magnetotail (e.g., Li et al. 2022) and in the solar wind (Wang et al. 2023), and could be caused by betatron acceleration.

The flow in the N direction exhibited a structured flow as well, with respect to the background flow of $-332\,\mathrm{km\,s^{-1}}$. The flow $\delta\ v_N$ was positive below the middle plane (left of the vertical dashed line in Figure 4) and became negative above the middle plane (right of the dashed line). Namely, the flow was moving toward the middle plane of the current layer from both sides, in accord with the reconnection inflowing. The inflowing speed of $\delta\ v_N$ was $\sim 10\,\mathrm{km\,s^{-1}}$ and then the reconnection rate v_{in}/v_A was estimated to be ∼0.14. Thus, this was a fast reconnection. The ion flows in the out-of-plane direction v_M were enhanced inside the current layer center. These out-of-plane ion flows have been extensively observed at the X-line in the magnetosphere (Nagai et al. 2001; Oieroset et al. 2001; R. S. Wang et al. 2020). Combining all the observations

mentioned above, we found that the PSP just crossed one reconnection ion diffusion region of Hall magnetic reconnection with a strong guide field. Therefore, fast Hall magnetic reconnection can occur in the solar wind as close as ∼0.26 au from the Sun.

It is challenging to estimate the spatial scale of this diffusion region in the solar wind via a single satellite. Assuming the diffusion region was propagating with a background flow in the L direction (135 km s^{-1}), we could estimate its length was 135 km s^{-1} × 8 s = 1080 km ∼ 69d_i where d_i is the ion inertial length. Then, the width of the diffusion region was ∼10d_i according to the estimated reconnection rate. The plasma heating was clear inside the ion diffusion region; however, it was much weaker than the reconnection at 1 au. The probable reason was that the time resolution of the PSP plasma data was still too low to resolve the diffusion region in detail.

About 6 minutes later, another reconnecting current layer was encountered by PSP at ∼08:31 UT (the rightmost vertical shaded area in Figure 2). It is displayed in the local current coordinate system in Figure 5, with $\boldsymbol{L} = [0.497,\ 0.285,\ 0.819]]$, $\boldsymbol{M} = [-0.232,\ 0.953,\ -0.191]$, and $\boldsymbol{N} = [-0.836,\ -0.095,\ 0.540]$ relative to the RTN coordinates. This local coordinate system is obtained from the same method as the previous event. $\boldsymbol{B}_1$ and $\boldsymbol{B}_2$ were the data at 08:30:55 and 08:31:17 UT at the two edges of the current layer. The MVA method was applied to the magnetic field during 0831:03–08:31:15 UT.

Within this current layer, there was also a strong shear flow (Figure 5(c)). The background flow was ∼205 km s^{-1} on the upside ($B_L > 0$, before 08:30:50 UT), which became ∼155 km s^{-1} on the downside ($B_L < 0$, after 08:31:10 UT). In the same way, assuming the flow varied smoothly across the layer, the background shear flow was added in Figure 5(c) (blue dashed curve). The background flows in the M and N directions were −105 and −298 km s^{-1}, respectively. Since the flows in three directions had quite different values, v_{pM} and v_{pN} minus their background flows, and v_{pL} plus −175 km s^{-1} were displayed evidently inside one panel (Figure 5(c)). As PSP crossed the current layer from one side to the other (B_L evolved from ∼50 nT at ∼08:30:50 UT to ∼−40 nT at ∼08:31:15 UT, Figure 5(b)), the proton flow v_L was first positive and then negative with respect to the background shear flow (Figure 5(c)). v_M was significantly intensified just at the center of the current layer. There was also a strong guide field in this event and the guide field was ∼40 nT, nearly equal to $|B_L|$ at the current layer edge. The magnetic field strength and plasma density exhibited clear asymmetry. The field strength was stronger above the middle plane of the current layer than below the middle plane (Figure 5(a)). On the contrary, the density (Figure 5(e)) was lower (∼180 cm^{-3}) above the middle plane than below the middle plane (∼230 cm^{-3}).

In the positive proton flow, B_M was positive initially, shortly dipped at 08:31:04 UT while PSP was still above the middle plane ($B_L > 0$), and then became positive again as PSP entered the region below the middle plane. Thus, we speculate that PSP passed through the second, first, and fourth quadrants of the ion diffusion region, as displayed in Figure 6(c). The Hall electric field pointed to the middle plane of the current layer was also detected inside the ion diffusion region (Figure 5(d)). v_N was negatively enhanced above the middle plane and positively enhanced below the plane near the current layer center, relative to the ambient flows of 298 km s^{-1}, in accord with the reconnection inflowing. Thus, the reconnection rate was estimated to be ∼0.2, where the inflowing speed of $\delta\ v_N$ was ∼15 km s^{-1}. Inside the ion diffusion region, the density sharply rose to 280 cm^{-3} at 08:30:06 UT (the vertical dashed line in Figure 5), which means that the plasma was trapped therein and the proton temperature did not show any significant enhancement (Figure 5(f)). The energetic electrons up to 604 eV were detected just after the diffusion region (Figure 5(g)).

Inside the ion diffusion region, a clear bipolar B_N was detected, accompanied with a small peak of B_M (Figure 5(b)), consistent with a magnetic flux rope. It is expanded in Figures 5(h) and (i). The density peak was just inside the flux rope. Therefore, the plasma was trapped inside the flux rope within the ion diffusion region. This flux rope should be moving along the $-L$ direction and thus was detected by PSP. This kind of small-scale flux rope observed inside the ion diffusion region was named a secondary magnetic flux rope (Wang et al. 2010a; Eastwood et al. 2016). A similar ion-scale magnetic flux rope in the solar wind current sheet has also been reported using Solar Orbiter observations in the solar wind current sheet (Eastwood et al. 2021). A secondary flux rope had been observed during reconnection in the magnetosphere and was regarded as an important factor for electron acceleration during reconnection (Wang et al. 2010a, 2010b; Zhao et al. 2019a; S. M. Wang et al. 2020; Zhong et al. 2020). This event was first reported by Phan et al. (2020), where the authors mainly studied the plasma flow in the R direction, focused on the negative reconnection jet, and neglected the positive flow. Here, we investigated the flows in all three directions, the Hall effect, and the small-scale magnetic flux ropes. Based on the comprehensive measurements of the PSP, we concluded that the spacecraft just crossed the ion diffusion region, other than just passing the reconnection exhaust.

5. Discussion and Conclusion

In this article, we investigated magnetic reconnection in one ICME during PSP Encounter 1. A few reconnection exhausts were previously observed inside the ICME (Phan et al. 2020) and two more reconnection exhausts were identified in its rear boundary region. Here, we mainly focused on direct observation of the reconnection diffusion region in the rear boundary region. The characteristics of the ion diffusion region included opposite sub-Alfvénic jets, out-of-plane flow, Hall electric field and magnetic field, and plasma heating inside the thin current layer. Flow reversal had been observed previously in the boundary regions of ICMEs (Wei et al. 2006) and was thought to be evidence for magnetic reconnection. Due to the relatively low sample rate of the Wind spacecraft, the opposite jets could not be explored in detail. Recently, the diffusion region of turbulent reconnection has been further examined in the solar wind at 1 au by MMS (Wang et al. 2023). Plenty of magnetic flux ropes and filamentary currents were detected inside the diffusion region, which plays an essential role in reconnection evolution to turbulence and in electron acceleration, as verified in the magnetosphere (R. S. Wang et al. 2016; S. M. Wang et al. 2020; Li et al. 2022).

In this article, we confirmed that the collisionless Hall magnetic reconnection can occur as close as 56R_S from the Sun. The characteristic of the reconnection in the solar wind is consistent with the observation in the magnetosphere. This means that knowledge of the Hall magnetic reconnection obtained from in situ measurements in the magnetosphere and

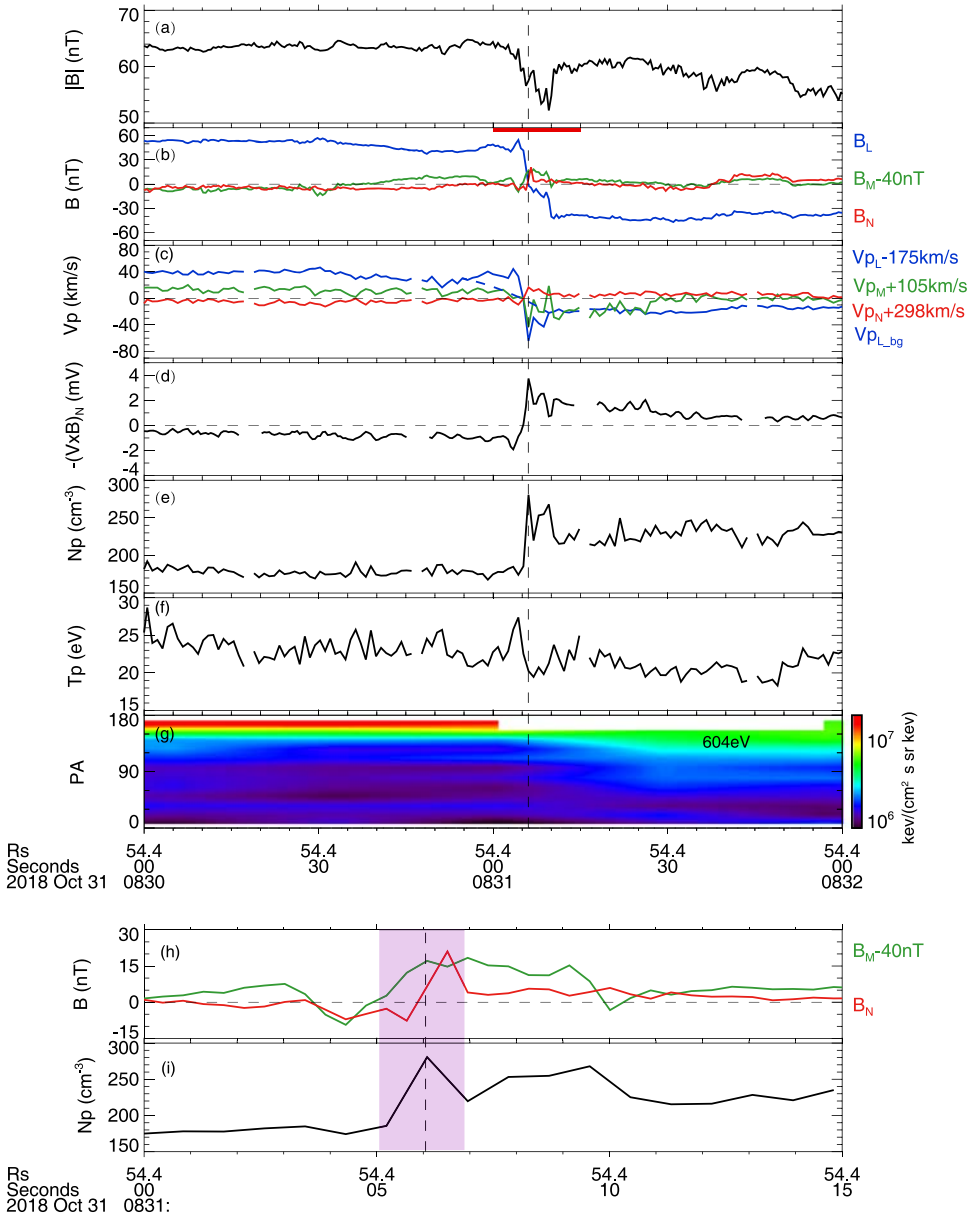

Figure 5. Observation of another ion diffusion region. Panels (a)–(g) show the data in the same format as Figure 3. The vertical dashed line denotes the B_L reversal point. The red bar at the top of (b) represents the time interval of the ion diffusion region. (h) Magnetic field components B_N(red), B_M(blue), and (i) proton number density.

from numerical simulations are also applicable in the solar wind. As PSP is gradually approaching the Sun in the following encounters, we can confirm whether the Hall magnetic reconnection is also therein, as well as its prevalence in the solar corona. Small-scale magnetic flux ropes or magnetic islands are frequently observed in interplanetary space (Moldwin et al. 2000; Cartwright & Moldwin 2008; Teh et al. 2009; Tian et al. 2010; Hu et al. 2018; Zhao et al. 2018, 2021; Wang et al. 2023).

The formation mechanisms of these small-scale flux ropes are still controversial. Some researchers suggested that these small-scale flux ropes are generated in the solar corona (Borovsky 2008; Feng & Wu 2009), like the ICME, and then are ejected from the Sun to interplanetary space. Alternatively, many researchers believe that the flux ropes are produced in interplanetary space due to local magnetic reconnection (Hu et al. 2018; Wang et al. 2023). Based on the MMS measurements in the solar wind, the flux ropes indeed can be formed in the local turbulent reconnection at ∼1 au. Here, we further found that the flux ropes are generated due to the local reconnection at ∼0.26 au. In the magnetosphere, the electrons can be efficiently accelerated inside the flux ropes (R.S. Wang et al. 2010a, 2010b; S.M. Wang et al. 2019, 2021). In the solar wind, energetic electrons have not been observed inside the ropes, which are larger than those reported in Figure 5. However, small-scale magnetic flux ropes have been proposed to explain the energetic charged particles (Zank et al. 2014; Zhao et al. 2018). The charged particles can be accelerated statistically in the region with numerous interacting flux ropes (Zhao et al. 2018, 2019b; Nakanotani et al. 2022). More effort is needed to resolve the exact roles of these small-scale flux ropes on energizing the charged particles.

In summary, magnetic reconnection is common inside the ICME reported here and in the interacting region between the

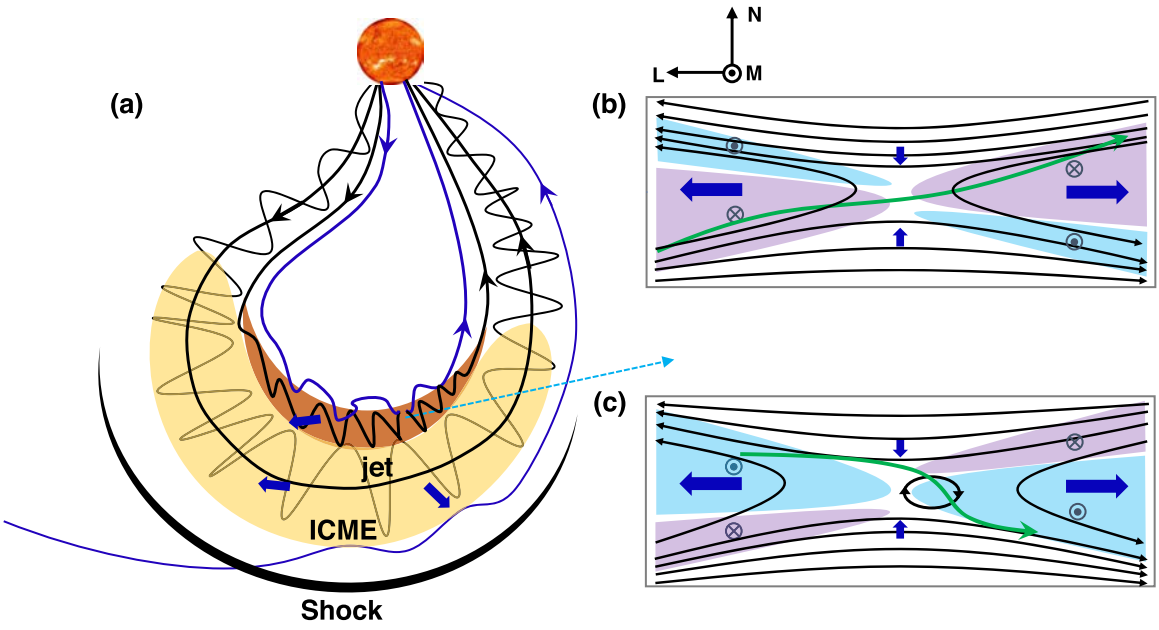

Figure 6. Schematic illustrations for (a) the magnetic cloud, and (b) and (c) the ion diffusion regions shown in Figure 4 and Figure 5, respectively.

ICME and the ambient solar wind. This means that magnetic reconnection can be triggered easily inside the solar wind and the stored magnetic free energy can be persistently released in interplanetary space.

This work is supported by the B-type Strategic Priority Program of the Chinese Academy of Sciences (XDB41000000, (R.W.)), the National Science Foundation of China (NSFC) grants (41922030 and 42174187, (R.W.)), the Key Research Program of Frontier Sciences CAS (QYZDJ-SSW-DQC010 (Q.L.)), and the Fundamental Research Funds for the Central Universities. Parker Solar Probe was designed, built, and is now operated by the Johns Hopkins Applied Physics Laboratory as part of NASA's Living with a Star (LWS) program (contract NNN06AA01C). Support from the LWS management and technical team has played a critical role in the success of the Parker Solar Probe mission. Thanks to the FIELDS team for providing data (PI: Stuart D. Bale, UC Berkeley). Thanks to the Solar Wind Electrons, Alphas, and Protons (SWEAP) team for providing data (PI: Justin Kasper, BWX Technologies).

ORCID iDs

Rongsheng Wang https://orcid.org/0000-0002-9511-7660
Yuming Wang https://orcid.org/0000-0002-8887-3919
Quanming Lu https://orcid.org/0000-0003-3041-2682
San Lu https://orcid.org/0000-0003-2248-5072

References

Alexander, D., Richardson, I. G., & Zurbuchen, T. H. 2006, SSRv, 123, 3
Bale, S. D., Badman, S. T., Bonnell, J. W., et al. 2019, Natur, 576, 237
Bale, S. D., Goetz, K., Harvey, P. R., et al. 2016, SSRv, 204, 49
Borovsky, J. E. 2008, JGRA, 113, A08110
Burch, J. L., Moore, T. E., Torbert, R. B., & Giles, B. L. 2016, SSRv, 199, 5
Burlaga, L., Sittler, E., Mariani, F., & Schwenn, R. 1981, JGR, 86, 6673
Cartwright, M. L., & Moldwin, M. B. 2008, JGR, 113, A09105
Case, A. W., Kasper, J. C., Stevens, M. L., et al. 2020, ApJS , 246, 43
Chen, P. F. 2011, LRSP, 8, 1
Dasso, S., Mandrini, C. H., Demoulin, P., & Luoni, M. L. 2006, A&A, 455, 349
Davis, M. S., Phan, T. D., Gosling, J. T., & Skoug, R. M. 2006, GeoRL, 33, L19102
Eastwood, J. P., Phan, T. D., Cassak, P. A., et al. 2016, GeoRL, 43, 4716
Eastwood, J. P., Phan, T. D., Oieroset, M., & Shay, M. A. 2010, JGRA, 115, A08215
Eastwood, J. P., Stawarz, J. E., Phan, T. D., et al. 2021, A&A, 656, A27
Feng, H. Q., & Wu, D. J. 2009, ApJ, 705, 1385
Fox, N. J., & McComas, D. J. 2016, SSRv, 204, 1
Fu, H. S., Vaivads, A., Khotyaintsev, Y. V., et al. 2017, GeoRL, 44, 37
Gopalswamy, N. 2006, SSRv, 124, 145
Gosling, J. T. 2012, SSRv, 172, 187
Gosling, J. T., Skoug, R. M., McComas, D. J., & Smith, C. W. 2005, JGRA, 110, A01107
Hu, Q., Zheng, J. L., Chen, Y., le Roux, J., & Zhao, L. L. 2018, ApJS, 239, 12
Ji, H. T., Daughton, W., & Jara-Almonte, J. 2022, NatRP, 4, 263
Kasper, J. C., Abiad, R., Austin, G., et al. 2016, SSRv, 204, 131
Kasper, J. C., Bale, S. D., Belcher , J. W., et al. 2019, Natur, 576, 228
Lavraud, B., Gosling, J. T., Rouillard, A. P., et al. 2009, SoPh, 256, 379
Lavraud, B., Ruffenach, A., & Rouillard, A. P. 2014, JGRA, 119, 26
Li, X. M., Wang, R. S., Lu, Q. M., et al. 2022, NatCo, 13, 3241
Lu, Q. M., Fu, H. S., Wang, R. S., & Lu, S. 2022, ChPhB, 31, 089401
Mistry, R., Eastwood, J. P., Phan, T. D., & Hietala, H. 2017, JGRA, 122, 5895
Moldwin, M. B., Ford, S., Lepping, R., Slavin, J., & Szabo, A. 2000, GeoRL, 27, 57
Nagai, T., Shinohara, I., & Fujimoto, M. 2001, JGR, 106, 25929
Nakamura, R., Baumjohann, W., Mouikis, C., et al. 2004, GeoRL, 31, L09804
Nakanotani, M., Zank , G. P., Zhao, L. L., et al. 2022, FrASS, 9, 954040
Oieroset, M., Phan, T. D., Fujimoto, M., Lin, R. P., & Lepping, R. P. 2001, Natur, 412, 414
Phan, T. D., Bale, S. D., Eastwood, J. P., et al. 2020, ApJS, 246, 34
Phan, T. D., Lavraud, B., Halekas, J. S., et al. 2021, A&A, 650, A13
Ruffenach, A., Lavraud, B., Owens, M. J., et al. 2012, JGRA, 117, A09101
Shen, C. L., Chi, Y. T., Wang, Y. M., Xu, M. J., & Wang, S. 2017, JGRA, 122, 5931
Shen, F., Feng, X. S., Wang, Y. M., et al. 2011, JGRA, 116, A09103
Teh, W. L., Sonnerup, B. U. O., Hu, Q., & Farrugia, C. J. 2009, AnGeo, 27, 807
Sonnerup, B. U. O. 1979, in Solar System Plasma Physics, ed. L. T. Lanzerotti, C. F. Kennel, & E. N. Parker (New York: North-Holland), 45
Sonnerup, B. U. Ö, & Cahill, L. J. 1967, JGR, 72, 171
Tian, H., Yao, S., Zong, Q. G., He, J. S., & Qi, Y. 2010, ApJ, 720, 454
Vasyliunas, V. M. 1975, RvGeo, 13, 303
Vörös, Z., Varsani, A., Yordanova, E., et al. 2021, JGRA, 126, e29415
Wang, R. S., Lu, Q. M., Du, A. M., & Wang, S. 2010a, PhRvL, 104, 175003

Wang, R. S., Lu, Q. M., Li, X., Huang, C., & Wang, S. 2010b, JGRA, 115, A11201
Wang, R. S., Lu, Q. M. , Lu, S., et al. 2020, GeoRL, 47, e88761
Wang, R. S., Lu, Q. M., Nakamura, R., et al. 2016, NatPh, 12, 263
Wang, R. S., Lu, Q.M., Nakamura, R., et al. 2018, GeoRL, 45, 4542
Wang, R. S., Nakamura, R., Lu, Q.M., et al. 2017, PhRvL, 118, 175101
Wang, R. S., Wang, S. M., Lu, Q. M., et al. 2023, NatAs, 7, 18
Wang, S. M., Wang, R. S., Lu, et al. 2019, JGRA, 126, 1753
Wang, S. M., Wang, R. S., Lu, Q. M., Fu, H. S., & Wang, S. 2020, NatCo, 11, 3964
Wang, S. M., Wang, R. S., Lu, Q. M., Russell, C. T., & Wang, S. 2021, JGRA, 124, e28860
Wang, Y. M., Shen, C. L., Liu, R., et al. 2018, JGRA, 123, 3238
Wang, Y. M., Ye, P. Z., & Wang, S. 2003, JGRA, 108, 1370
Wang, Y. M., Ye, P. Z., Wang, S., Zhou, G. P., & Wang, J. X. 2002, JGRA, 107, 1340
Wang, Y. M., Zheng, H., Wang, S., & Ye, P. 2005, A&A, 434, 309
Wei, F. S., Feng, X. S., Yang, F., & Zhong, D. K. 2006, JGRA, 111, A03102
Wei, F. S., Hu, Q., Feng, X. S., & Fan, Q. L. 2003, SSRv, 107, 107
Whittlesey, P. L., Larson, D. E., Kasper, J. C., et al. 2020, ApJS, 246, 74
Xiong, M., Zheng, H., Wu, S. T., Wang, Y. M., & Wang, S. 2007, JGRA, 112, A11103
Xu, X., Wei, F., & Feng, X. 2011, JGRA, 116, A05105
Xue, X., Wei, F. S., Feng, X. S., Wang, S., & Xiong, M. 2005, P&SS, 53, 443
Zank, G. L., le Roux, J. A., Webb , G. M., Dosch, A., & Khabarova, O. 2014, ApJ, 797, 28
Zhang, J., Richardson, I. G., Webb, D. F., et al. 2007, JGRA, 112, A10102
Zhao, L. L., Zank, G. P., Adhikari, L., et al. 2020, ApJS, 246, 26
Zhao, L. L., Zank, G. P., Chen, Y., et al. 2019a, ApJ, 872, 4
Zhao, L. L., Zank, G. P., Hu, Q., et al. 2019b, ApJ, 886, 144
Zhao, L. L., Zank, G. P., Hu, Q., et al. 2021, A&A, 650, A12
Zhao, L.-L., Zank, G. P., Khabarova, O., et al. 2018, ApJL, 864, L34
Zhong, Z. H., Zhou, M., Tang, R. X. , et al. 2020, GeoRL, 47, e85141
Zurbuchen, T. H., & Richardson, I. G. 2006, SSRv, 123, 31